Constraints on the orbit of the young substellar companion GQ Lup B from high-resolution spectroscopy and VLTI/GRAVITY astrometry

Venkatesan, V.; Blunt, S.; Wang, J.J.; Lacour, S.; Marleau, G.-D.; Coleman, G.A.L.; ... ; Exogravity Collaboration

The Astrophysical Journal, 993:69 (12pp), 2025 November 1 https://doi.org/10.3847/1538-4357/ae0c15

Constraints on the Orbit of the Young Substellar Companion GQ Lup B from High-resolution Spectroscopy and VLTI/GRAVITY Astrometry*

Vidya Venkatesan[1,42], S. Blunt[2], J. J. Wang[3], S. Lacour[4,5], G.-D. Marleau[6,7,8], G. A. L. Coleman[9], L. Guerrero[10], W. O. Balmer[11,12], L. Pueyo[12], T. Stolker[13], J. Kammerer[5], N. Pourré[14], M. Nowak[15], E. Rickman[16], A. Sivaramakrishnan[11,12], D. Sing[11,17], K. Wagner[18], A.-M. Lagrange[4,14], R. Abuter[5], A. Amorim[19,20], R. Asensio-Torres[7], J.-P. Berger[14], H. Beust[14], A. Boccaletti[4], M. Bonnefoy[14], H. Bonnet[5], M. S. Bordoni[21], G. Bourdarot[21], W. Brandner[7], F. Cantalloube[22], P. Caselli[21], B. Charnay[4], G. Chauvin[23], A. Chavez[3], A. Chomez[4,14], E. Choquet[22], V. Christiaens[24], Y. Clénet[4], V. Coudé du Foresto[4], A. Cridland[13], R. Davies[21], R. Dembet[4], J. Dexter[25], A. Drescher[21], G. Duvert[14], A. Eckart[26,27], F. Eisenhauer[21], N. M. Förster Schreiber[21], P. Garcia[20,28], R. Garcia Lopez[7,29], E. Gendron[4], R. Genzel[21,30], S. Gillessen[21], J. H. Girard[12], S. Grant[21], X. Haubois[31], G. Heissel[4,32], Th. Henning[7], S. Hinkley[33], S. Hippler[7], M. Houllé[14], Z. Hubert[14], L. Jocou[14], M. Keppler[7], P. Kervella[4], L. Kreidberg[7], N. T. Kurtovic[21], V. Lapeyrère[4], J.-B. Le Bouquin[14], D. Lutz[21], A.-L. Maire[14], F. Mang[21], A. Mérand[5], C. Mordasini[34,35], D. Mouillet[14], E. Nasedkin[7], T. Ott[21], G. P. P. L. Otten[36], C. Paladini[31], T. Paumard[4], K. Perraut[14], G. Perrin[4], S. Petrus[37], O. Pfuhl[5], D. C. Ribeiro[21], Z. Rustamkulov[17], J. Shangguan[38], T. Shimizu[21], A. Shields[1], J. Stadler[39,40], O. Straub[40], C. Straubmeier[41], E. Sturm[21], L. J. Tacconi[21], A. Vigan[22], F. Vincent[4], S. D. von Fellenberg[27], F. Widmann[21], T. O. Winterhalder[5], J. Woillez[5], S. Yazici[21], and the ExoGRAVITY Collaboration

[1] Department of Physics and Astronomy, University of California, Irvine, CA, USA
[2] Department of Physics and Astronomy, University of California, Santa Cruz, CA, USA
[3] Center for Interdisciplinary Exploration and Research in Astrophysics (CIERA) and Department of Physics and Astronomy, Northwestern University, Evanston, IL 60208, USA
[4] LIRA, Observatoire de Paris, Université PSL, Sorbonne Université, Université Paris Cité, CY Cergy Paris Université, CNRS, 92190 Meudon, France
[5] European Southern Observatory, Karl-Schwarzschild-Straße 2, 85748 Garching, Germany
[6] Division of Space Research & Planetary Sciences, Physics Institute, University of Bern, Sidlerstr. 5, 3012 Bern, Switzerland
[7] Max-Planck-Institut für Astronomie, Königstuhl 17, 69117 Heidelberg, Germany
[8] Fakultät für Physik, Universität Duisburg-Essen, Lotharstraße 1, 47057 Duisburg, Germany
[9] Astronomy Unit, Department of Physics and Astronomy, Queen Mary University of London, Mile End Road, London, E1 4NS, UK
[10] Department of Physics and Astronomy, Northwestern University, Evanston, IL 60208, USA
[11] Department of Physics & Astronomy, Johns Hopkins University, 3400 N. Charles Street, Baltimore, MD 21218, USA
[12] Space Telescope Science Institute, 3700 San Martin Drive, Baltimore, MD 21218, USA
[13] Leiden Observatory, Leiden University, P.O. Box 9513, 2300 RA Leiden, The Netherlands
[14] Université Grenoble Alpes, CNRS, IPAG, 38000 Grenoble, France
[15] Institute of Astronomy, University of Cambridge, Madingley Road, Cambridge CB3 0HA, UK
[16] European Space Agency (ESA), ESA Office, Space Telescope Science Institute, 3700 San Martin Drive, Baltimore, MD 21218, USA
[17] Department of Earth & Planetary Sciences, Johns Hopkins University, Baltimore, MD, USA
[18] Department of Astronomy and Steward Observatory, University of Arizona, 933 N Cherry Avenue, Tucson, AZ 85712, USA
[19] Universidade de Lisboa—Faculdade de Ciências, Campo Grande, 1749-016 Lisboa, Portugal
[20] CENTRA—Centro de Astrofísica e Gravitação, IST, Universidade de Lisboa, 1049-001 Lisboa, Portugal
[21] Max-Planck-Institut für extraterrestrische Physik, Gießenbachstraße 1, 85748 Garching, Germany
[22] Aix Marseille Univ, CNRS, CNES, LAM, Marseille, France
[23] Université Côte d'Azur, Observatoire de la Côte d'Azur, CNRS, Laboratoire Lagrange, Bd de l'Observatoire, CS 34229, 06304 Nice cedex 4, France
[24] STAR Institute, Université de Liège, Allée du Six Août 19c, 4000 Liège, Belgium
[25] Department of Astrophysical & Planetary Sciences, JILA, Duane Physics Bldg., 2000 Colorado Avenue, University of Colorado, Boulder, CO 80309, USA
[26] I. Physikalisches Institut, Universität zu Köln, Zülpicher Straße 77, 50937 Cologne, Germany
[27] Max-Planck-Institut für Radioastronomie, Auf dem Hügel 69, 53121 Bonn, Germany
[28] Universidade do Porto, Faculdade de Engenharia, Rua Dr. RobertoRua Dr. Roberto Frias, 4200-465 Porto, Portugal
[29] School of Physics, University College Dublin, Belfield, Dublin 4, Ireland
[30] Departments of Physics and Astronomy, Le Conte Hall, University of California, Berkeley, CA 94720, USA
[31] European Southern Observatory, Casilla 19001, Santiago 19, Chile
[32] Advanced Concepts Team, European Space Agency, TEC-SF, ESTEC, Keplerlaan 1, NL-2201, AZ Noordwijk, The Netherlands
[33] University of Exeter, Physics Building, Stocker Road, Exeter EX4 4QL, UK
[34] Division of Space Research & Planetary Sciences, Physics Institute, University of Bern, Gesellschaftsstr. 6, 3012 Bern, Switzerland
[35] Center for Space and Habitability, Universität Bern, Gesellschaftsstr. 6, 3012 Bern, Switzerland
[36] Academia Sinica, Institute of Astronomy and Astrophysics, 11F Astronomy-Mathematics Building, NTU/AS campus, No. 1, Section 4, Roosevelt Road, Taipei 10617, Taiwan
[37] NASA-Goddard Space Flight Center, 8800 Greenbelt Road, Greenbelt, MD 20771, USA
[38] The Kavli Institute for Astronomy and Astrophysics, Peking University, Beijing 100871, People's Republic of China
[39] Max-Planck-Institut für Astrophysik, Karl-Schwarzschild-Straße 1, 85741 Garching, Germany
[40] Excellence Cluster ORIGINS, Boltzmannstraße 2, D-85748 Garching bei München, Germany

* Based on observations collected at the European Southern Observatory under ESO programmes 1104.C-0651 and 109.238N.001.

[41] 1st Institute of Physics, University of Cologne, Zülpicher Straße 77, 50937 Cologne, Germany
Received 2025 August 4; revised 2025 September 24; accepted 2025 September 24; published 2025 October 24

Abstract

Understanding the orbits of giant planets is critical for testing planet formation models, particularly at wide separations (>10 au) where traditional core accretion becomes inefficient. However, constraining orbits at these separations has historically been challenging due to sparse orbital coverage and related degeneracies in the orbital parameters. In this work, we use existing high-resolution ($R \sim 100{,}000$) spectroscopic measurements from CRIRES+, astrometric data from SPHERE, NACO, and Atacama Large Millimeter/submillimeter Array, and combine it with new high-precision GRAVITY astrometry data to refine the orbit of GQ Lup B, a $\sim$30 M_J companion at $\sim$100 au, in a system that also hosts a circumstellar disk and a wide companion, GQ Lup C. Including radial velocity (RV) data significantly improves orbital constraints by breaking the degeneracy between inclination and eccentricity that plagues astrometry-only fits for long-period companions. Our work is one of the first to combine high-precision astrometry with the companion's relative radial velocity measurements to achieve significantly improved orbital constraints. The eccentricity is refined from $e = 0.47^{+0.14}_{-0.16}$ (GRAVITY only) to $e = 0.35^{+0.10}_{-0.09}$ when RVs and GRAVITY data are combined. We also compute the mutual inclinations between the orbit of GQ Lup B, the circumstellar disk, the stellar spin axis, and the disk of GQ Lup C. The orbit is misaligned by 63^{+6}_{-14}° relative to the circumstellar disk, 52^{+19}_{-24}° with the host star's spin axis, but appears more consistent (34^{+6}_{-13}°) with the inclination of the wide tertiary companion GQ Lup C's disk. These results support a formation scenario for GQ Lup B consistent with cloud fragmentation. They highlight the power of combining companion RV constraints with interferometric astrometry to probe the dynamics and formation of wide-orbit substellar companions.

Unified Astronomy Thesaurus concepts: Exoplanet formation (492); Orbits (1184)

1. Introduction

One of the fundamental puzzles in exoplanetary science is the formation and evolution of giant planets and substellar companions at wide separations (tens to hundreds of astronomical units away from their host stars). At such distances, the traditional core accretion theory struggles to explain the formation of a planetary core massive enough to trigger runaway gas accretion before the dissipation of the protoplanetary disk (J. B. Pollack et al. 1996; S. Inaba et al. 2003; M. Ikoma & H. Kobayashi 2025). Gravitational instability in the disk is one alternative formation pathway that consists of massive clump formation at >100 au (A. P. Boss 1997; L. Mayer et al. 2002), followed by inward migration and potential disruption (K. Kratter & G. Lodato 2016; S. Nayakshin 2017). Alternative scenarios such as dynamical scattering (D. Veras et al. 2009), outward migration via disk–planet interactions (A. Crida et al. 2009), and direct collapse out of a molecular cloud (D. Stamatellos et al. 2007; D. Stamatellos & A. P. Whitworth 2009) have also been proposed. Each pathway is expected to leave a unique imprint on a system's dynamical architecture, particularly in orbital eccentricities (G.-D. Marleau et al. 2019), mutual inclinations (difference in orbital angular momentum vector orientations of planets in the same system; R. J. De Rosa et al. 2020), and spin–orbit obliquities (difference in vector orientations of stellar spin axes and planetary orbit; M. L. Bryan et al. 2021; B. P. Bowler et al. 2023). Therefore, constraining the orbits of exoplanets with limited astrometric temporal baselines may be key to uncovering the formation mechanisms of widely separated objects. However, for most wide-orbit companions, these dynamical signatures remain poorly constrained due to long orbital periods, typically 1000+ yr, and corresponding limited observational baselines.

The GQ Lup system is located in the Lupus star-forming region approximately 151 pc away (Gaia Collaboration et al. 2023), and consists of a young (<2–5 Myr) (J. F. Donati et al. 2012; H. Schwarz et al. 2016; T. Stolker et al. 2021) K7 T Tauri star, a transition disk extending to $\sim$50 au (M. A. MacGregor et al. 2017; Y.-L. Wu et al. 2017), and a directly imaged substellar companion, GQ Lup B. One of the first directly imaged substellar companions (R. Neuhauser et al. 2005), with a projected separation of $\sim$100 au and an orbital period of $\sim$900–1200 yr (T. Stolker et al. 2021), GQ Lup B has an estimated mass between 10 and 40 M_J (T. Stolker et al. 2021), placing it near the planet/brown dwarf boundary (which may occur around 15–40 M_J based on features in the stellar mass function; G. Chabrier 2003; M. Reggiani et al. 2016; A. T. Stevenson et al. 2023). In addition to GQ Lup B, the system hosts a likely wide tertiary companion, GQ Lup C, identified by C. Lazzoni et al. (2020) and J. M. Alcalá et al. (2020), at a projected separation of $\sim$2400 au. Its bound status remains uncertain, but such a distant companion could play a role in the long-term dynamical evolution of the system. With two companions at wide separations and the presence of a circumstellar disk, this system offers a valuable laboratory to investigate the formation and evolution of widely separated objects.

Current observational evidence from GQ Lup B's atmosphere supports a formation scenario via disk instability or direct collapse. High-resolution spectroscopic studies have revealed CO and H_2O absorption features in its atmosphere (H. Schwarz et al. 2016), and its carbon isotopic ratio and C/O ratio are consistent with those of the host star (J. W. Xuan et al. 2024; D. González Picos et al. 2025), favoring a common origin and suggesting formation from the same protostellar disk or via gravoturbulent fragmentation of a single molecular cloud. Moreover, detection of strong Hα emission indicates that the planet is still accreting (C. Marois et al. 2007), and the possible presence of a circumplanetary disk (G. Cugno et al.

[42] NASA FINESST Fellow.

Table 1
Astrometric Measurements for GQ Lup B

MJD	Seperation (mas)	Uncertainty (mas)	P.A. (deg)	Unc. (deg)	Instrument
49445	713.8	35.5	275.5	1.1	ESO 3.6 ComeOn+[a]
51279	739	11	275.62	0.86	HST/WFPC2[a]
53182	732.5	3.4	275.45	0.30	VLT/NACO[a]
57128	721.0	3.0	277.6	4.0	ALMA[b]
58345.1	711.6	2.4	278.27	0.24	SPHERE[b]
58551.3	720.3	3.4	277.9	0.18	NACO[c]
58557.2	715.0	2.8	277.82	0.17	NACO[c]
58593.1	701.0	20.0	278.3	1.2	MUSE[c]

Notes.
[a] M. Janson et al. (2006).
[b] Y.-L. Wu et al. (2017).
[c] T. Stolker et al. (2021).

2024) further supports the interpretation of GQ Lup B as a young, evolving system with the potential for satellite formation and continued dynamical evolution.

In addition to the atmospheric composition, orbital architecture offers a complementary avenue for probing the origins of substellar companions (e.g., J. W. Xuan et al. 2022). Precise orbital parameters—particularly eccentricity—can help differentiate between formation scenarios, since high eccentricity can indicate scattering (M. L. Bryan et al. 2016; R. Dong et al. 2016), while low eccentricity can imply disk driven migration, or in situ formation consistent with the overall eccentricity distribution of directly imaged planets (B. P. Bowler et al. 2020; C. R. Do Ó et al. 2023; V. Nagpal et al. 2023). Historically, the orbital characterization of directly imaged planets has relied almost exclusively on relative astrometry, limiting our ability to tightly constrain orbital elements—particularly eccentricity and inclination. However, widely separated systems like GQ Lup B pose a challenge for traditional orbit-fitting techniques due to their long orbital periods. For this companion, only about 0.5% of the full orbit is currently sampled by the astrometric baseline, limiting the precision with which its orbital parameters can be constrained. This limitation is amplified for long-period companions like GQ Lup B, where current astrometric baselines cover only a small fraction of the orbit, and measurements from absolute astrometry with Hipparcos and/or Gaia are unconstraining. A key challenge in such cases is the well-known degeneracy between eccentricity and inclination (R. Ferrer-Chávez et al. 2021), where nearly circular, edge-on orbits can be difficult to distinguish from more eccentric, more face-on configurations based solely on sky-projected motion. Incorporating high-precision relative radial velocity (RV) data, even over a relatively short baseline, can help break this degeneracy. Rather than waiting decades to detect orbital curvature via astrometry alone, precise RV measurements can improve constraints (S. Blunt et al. 2023).

The advent of high-precision astrometry from instruments like GRAVITY (S. Lacour et al., 2020) has enabled robust orbital constraints for directly imaged companions, including HIP99770 b (T. O. Winterhalder et al. 2025), HD136164 Ab—an eccentric brown dwarf likely formed via fragmentation (W. O. Balmer et al. 2024)—AF Lep b, whose circular orbit is consistent with a core accretion scenario (W. O. Balmer et al. 2025), and YSES1 b (J. Roberts et al. 2024, in preparation). Earlier efforts also demonstrated GRAVITY's power in systems such as HD206893 b (J. Kammerer et al. 2021) and β Pic b (GRAVITY Collaboration et al. 2020; G. M. Brandt et al. 2021). This progress is further complemented by advances in high-resolution spectroscopy. Instruments like CRIRES+ can now allow us to place a slit directly on GQ Lup B and extract planetary RV. This technique, long a cornerstone of stellar orbital characterization, is now viable for planets on wide separation from their host stars and with favorable contrasts.

While T. Stolker et al. (2021) combined RV data with Very Large Telescope (VLT)/NACO and VLT/MUSE astrometry, the low-precision measurements resulted in large uncertainties. This study combines multiepoch astrometric measurements, including new high-resolution astrometry from the GRAVITY instrument, with recent planetary RV measurements derived from the spectrum of GQ Lup B itself to refine the orbital parameters of the companion and assess their implications for its formation. In addition to refining the orbital parameters of GQ Lup B, this work evaluates the relative information content of the available observational datasets, focusing on relative astrometry and relative RVs, in constraining GQ Lup B's orbit. These orbit fitting methods are also directly relevant to the science goals of future missions such as the Habitable Worlds Observatory (HWO; NASA HWO STDT 2023). In particular, this technique of combining high-precision astrometry with relative RVs to break the degeneracies between inclination and eccentricity could potentially be adapted to HWO rocky planets. In addition to gaining insights into the formation and dynamical history of the system, accurate orbital solutions are also critical for determining key parameters (e.g., orbital phase and stellar irradiation) that inform climate modeling and habitability assessments for eccentric rocky planets with HWO (V. Venkatesan et al. 2025).

The paper is structured as follows. Section 2 describes the data acquisition and inputs used in `orbitize!`. Section 3 outlines our orbit-fitting methodology and the calculation of orbital eccentricity using both RV and astrometric data. The results are presented in Section 4 and discussed in Section 5. Finally, we summarize our conclusions in Section 6.

2. Data

We used a combination of astrometric data and low-precision and high-precision RV data for GQ Lup B from various sources. In this paper, we present four new epochs of VLTI/GRAVITYastrometry, described in Section 2.1, and also supplement this data with literature astrometry from Hubble Space Telescope (HST), Atacama Large Millimeter/submillimeter Array (ALMA), SPHERE, NACO, and MUSE, as mentioned in Table 1, to extend the time baseline.

2.1. Gravity Data

We observed GQ Lup B with GRAVITY at four different epochs. We used the instrument with combined polarization and medium resolution ($R \approx 400$). The log of the observations is given in Table 2. During the night of 2021 August 27, we used GRAVITY on the 8 m Unit Telescopes (UT), while during the other three nights, we used the 1.8 m

Table 2
Observation Log for GQ Lup

Object	Date	Start (UT)	End (UT)	Detector Integration Time/NDIT/NEXP (s)/⋯/⋯	Airmass	τ_0 (ms)	Seeing (arcsec)	Axis	Station
GQLup B	2021-08-27	23:16:16	23:25:04	30.0 s/16/2	1.1/1.1	3.0/6.8	0.62/0.73	OFF-AXIS	UTs
HD174536 AB	2021-08-27	23:46:32	23:59:51	3.0 s/12/4	1.0/1.1	4.9/6.6	0.64/0.93	OFF-AXIS	UTs
GQLup AB	2022-08-14	00:48:23	01:31:26	100.0 s/4/4	1.1/1.2	2.5/5.0	0.52/0.67	ON-AXIS	ATs
GQLup AB	2022-09-06	00:11:39	00:50:29	100.0 s/4/4	1.2/1.4	3.8/5.8	0.58/1.17	ON-AXIS	ATs
GQLup AB	2023-03-19	05:48:15	06:20:36	100.0 s/4/3	1.2/1.3	4.8/6.5	0.88/1.17	ON-AXIS	ATs

Auxiliary Telescopes (AT). When observing with the UTs, the large separation ($\geqslant 0\farcs6$) prevented us from using the ON-AXIS mode. Therefore, we used the OFF-AXIS mode and a binary star to calibrate the metrology. This binary was HD17453 (M. Nowak et al. 2024), a system with a contrast of 40 and a separation of $1\farcs5$. During the four other observation campaigns, we used the ON-AXIS mode and therefore the star itself (GQ Lup A) for metrology referencing. The data were preprocessed by the official ESO GRAVITY pipeline,[43] yielding uncalibrated intermediary data products called `astrored`. This product was then fed into a set of GRAVITY consortium Python scripts, `run_gravi_astrored_astrometry`[44] to obtain spectra and astrometry for each epoch. We note that this paper focuses only on the astrometry, while the spectra will be published in a separate paper (Kammerer et al. 2025, in preparation).

A summary of the literature astrometry is presented in Table 1, while the new GRAVITY astrometry is provided in Table 3.

Table 3
New GRAVITY Astrometric Constraints for GQ Lup B

Epoch (MJD)	R.A. Offset (mas)	R.A. Unc. (mas)	Decl. Offset (mas)	Decl. Unc. (mas)	R.A./Decl. Correlation
60022.256	−698.969	0.055	114.058	0.153	−0.843
59828.023	−699.789	0.060	112.615	0.057	0.652
59805.051	−699.876	0.044	112.491	0.062	0.796
59453.975	−702.069	0.027	110.363	0.057	0.208

2.2. *Crires+ Data*

High-precision RV data were taken from D. González Picos et al. (2025), who report a companion velocity of

$$v_B = 2.03 \pm 0.04 \text{ km s}^{-1},$$

measured using the upgraded CRIRES+ instrument on VLT. CRIRES+ offers approximately 10 times broader *K*-band coverage (0.95–5.3 μm), significantly higher throughput, and resolving power ($R \gtrsim 100{,}000$; M. Holmberg & N. Madhusudhan 2022), as compared to CRIRES.

This value agrees with the earlier, lower-precision RV value of (H. Schwarz et al. 2016)

$$v_B = 2.0 \pm 0.4 \text{ km s}^{-1},$$

taken with CRIRES. The larger uncertainty in that result was driven not only by narrower wavelength coverage but also by lower throughput and signal to noise, yielding 20–30 in companion spectra only after long exposures. Therefore, the enhanced RV precision reported in D. González Picos et al. (2025) reflects both the broadened spectral coverage of CRIRES+ and its significantly improved throughput and data quality. However, D. González Picos et al. (2025) acknowledge that their reported uncertainty does not account for additional observed variability in the host star's RV, estimated by J. F. Donati et al. (2012), to be at the level of 0.4 km s^{-1} between 2009 and 2011. Instrumental effects, intense magnetic stellar activity on the young host star, accretion-driven RV jitter, or an additional unresolved companion in the system may explain this variability. Given this, the RV uncertainty reported in D. González Picos et al. (2025) likely underestimates the true error budget. Additionally, recent work by K. Horstman et al. (2024) demonstrates the application of this technique to GQ Lup B, using high-resolution KPIC spectroscopy to measure the absolute RVs and search for exomoon-induced modulations. Since the analysis is focused on the planet's RV alone, rather than the relative RV of the planet and the host star, it is more susceptible to instrumental systematics. They report RV variability at the ∼400–1000 m s^{-1} level, which likely reflects the precision limits of KPIC rather than confirmed RV variability. This highlights the challenges of extracting high-precision RVs from directly imaged companions and the need for caution when interpreting such measurements. Given the potential for significant astrophysical variability not reflected in the formal error budget of the high-precision CRIRES+ measurements, we adopt the relative RV value from CRIRES (H. Schwarz et al. 2016) in our analysis, while also exploring how the higher-precision CRIRES+ RV might further constrain the eccentricity of the system. Although the CRIRES measurement is less precise, it benefits from being a differential RV—measuring the planet's velocity relative to the host star—using spectra taken simultaneously. This approach helps mitigate the impact of instrumental systematics, as shared systematics between the star and planet spectra are largely canceled out. However, if CRIRES introduces variability on timescales shorter than the observation itself (e.g., subexposure level), such effects could still influence the measurement. Investigating such potential systematics will be an important direction for future work. In the meantime, we conservatively adopt the

[43] Available at https://www.eso.org/sci/software/pipelines/gravity/gravity-pipe-recipes.html.
[44] Developed in the context of the ExoGRAVITY large program, and available at https://version-lesia.obspm.fr/repos/DRS_gravity/gravi_tools3/.

Table 4
Radial Velocity Measurements of GQ Lup B

Epoch (MJD)	RV (km s^{-1})	Unc. (km s^{-1})	Instrument
60003	2.03	±0.04	CRIRES+[a]
56806	2.0	±0.4	CRIRES[b]

Notes.
[a] D. González Picos et al. (2025).
[b] H. Schwarz et al. (2016).

CRIRES value for our baseline analysis. The RV measurements are listed in Table 4.

3. Orbit Analysis

We used `orbitize!` (S. Blunt et al. 2020) to perform six distinct orbit fits using various combinations of RV and astrometric data. These configurations were designed to evaluate each dataset's individual and combined contributions to the final orbital constraints. The six explored cases are shown in Table 5. These combinations were chosen to isolate the effects of GRAVITY astrometry and the precision of the RV data on breaking degeneracies in key orbital elements, such as inclination and eccentricity.

All fits used the following orbital parameters as the model basis: semimajor axis (a), eccentricity (e), inclination (i; where $i = 0°$ corresponds to a face-on orbit), argument of periastron of the companion (ω_P), position angle of nodes (Ω), and the epoch of periastron passage τ, parameterized as a fraction of the orbital period past a reference epoch, defined to be 58849 MJD. We adopted identical uniform priors for all six fits, following S. Blunt et al. (2020). We performed all orbital fits using the parallel-tempered implementation of the affine-invariant Markov Chain Monte Carlo sampler `ptemcee` (D. Foreman-Mackey et al. 2013; W. D. Vousden et al. 2016). For each run, we used 20 temperatures and 1000 walkers. For the fits incorporating RVs or GRAVITY constraints, including the `GRAVNoRV`, `GRAVLowRV`, and `GRAVHighRV` cases (see Table 5), we ran the sampler for 200,000 total steps, following an initial burn-in phase of 100,000 steps. For the `NoGRAVNoRV`, `NoGRAVLowRV`, and `NoGRAVHighRV` fits, we used a shorter chain length of 50,000 steps, with 10,000 steps for burn-in. In all cases, every 100th step was saved, and the posterior samples were taken from the post-burn-in portion of each walker's chain. Convergence was assessed by eye.

We imposed Gaussian priors on the total system mass and parallax, with values of $M = 1.05 \pm 0.07 M_\odot$ (H. Schwarz et al. 2016) and $\pi = 6.489 \pm 0.029$ mas (Gaia Collaboration et al. 2023). These parameters do not strongly correlate with any other orbital elements in the posterior, and their marginalized posteriors closely reproduce the imposed priors.

Figures 1 and 2 show one example of the orbit fitting results from case `GravLowRV`. The orbit plot displays 100 orbital solutions drawn from the posterior, projected onto the sky. The color gradient encodes time, showing the evolution of the planet's apparent motion. Red points on the right indicate the astrometric data points, and the time evolution of the projected separation angle and position angle is shown in gray. The corner plot displays marginalized 1D and 2D posterior samples for the eight fitted orbital parameters for case `GravLowRV`.

4. Results

Our orbit fits reveal that including GRAVITY astrometry substantially improves constraints on the eccentricity and inclination of GQ Lup B, as shown in Figure 3. Without GRAVITY data (cases `NoGRAVNoRV`, `NoGRAVLowRV`, and `NoGRAVHighRV`), the eccentricity posteriors are broad and weakly constrained, offering limited insight into the eccentricity of the orbit. In contrast, the GRAVITY-only astrometry case (`GRAVNoRV`) imposes a strong upper limit on the eccentricity, significantly tightening the distribution even to $e = 0.47^{+0.14}_{-0.16}$ even in the absence of RV data, although some inclination–eccentricity degeneracy remains.

Incorporating RV data further refines the planet's orbital eccentricity. We adopt the lower-precision measurement from H. Schwarz et al. (2016), as the higher-precision dataset may be affected by unmodeled stellar variability or an unresolved companion (see Section 2). With the H. Schwarz et al. (2016) RV included, we obtain $e = 0.35^{+0.10}_{-0.09}$. Although using the high-precision RV data yields a tighter peak at $e = 0.20^{+0.14}_{-0.06}$, we treat this value with caution and base our analysis on the more conservative solution from the lower-precision measurement. Similarly, the inclination constraints, visible in the lower panels of Figure 3, are broad, assuming only the literature astrometry, spanning from nearly face-on to significantly inclined orbits. However, with GRAVITY astrometry alone, the inclination peaks at $44^{+6.42°}_{-9.62°}$. Adding the low-precision RV data refines the value further, resulting in a more sharply peaked inclination posterior at $48^{+3.7°}_{-4.9°}$. Including the high-precision RV sharpens the distribution even more, yielding a peak at $56^{+1.5°}_{-4.3°}$, although we adopt the value derived from the low-precision data for this study as previously stated. The posterior median along with the 1 σ uncertainties for all six cases are provided in Table 6.

Figure 4 presents the joint posterior distributions of eccentricity and inclination for GQ Lup B across four modeling configurations: `NoGRAVNoRV`, `GRAVNoRV`, `GravLowRV`, and `GravHighRV`. Contours represent the 1σ and 2σ confidence regions. Including GRAVITY data significantly reduces the volume of the eccentricity–inclination posterior, but a strong degeneracy between the two parameters is still apparent. Including the relative RVs, on the other hand, reduces the degeneracy itself. The `GRAVLowRV` configuration, our adopted case, yields a well-localized, unimodal posterior consistent with a moderately eccentric orbit.

Figure 5 presents the posterior distribution of the orbital inclination, longitude of ascending node (Ω), and 3-D mutual inclination between GQ Lup B and the star, the circumstellar disk, and the disk of GQ Lup C. In the top panel, the inclination constraints obtained from our adopted case, $\sim 48^{+3.7°}_{-4.9°}$, are compared against the inclination of the circumstellar disk ($\sim 60° \pm 0.5$; M. A. MacGregor et al. 2017), the stellar spin axis ($\sim 27° \pm 5°$; C. Broeg et al. 2007), and the disk of GQ Lup C ($\sim 44° \pm 2°$; C. Lazzoni et al. 2020). The planet's orbital inclination appears roughly consistent with that of GQ Lup C's disk.

In the middle panel, the longitude of the ascending node (Ω) is strongly constrained for GQ Lup B at $257^{+7.5°}_{-5.1°}$, and appears offset from both the disk of GQ Lup C disk, which peaks at

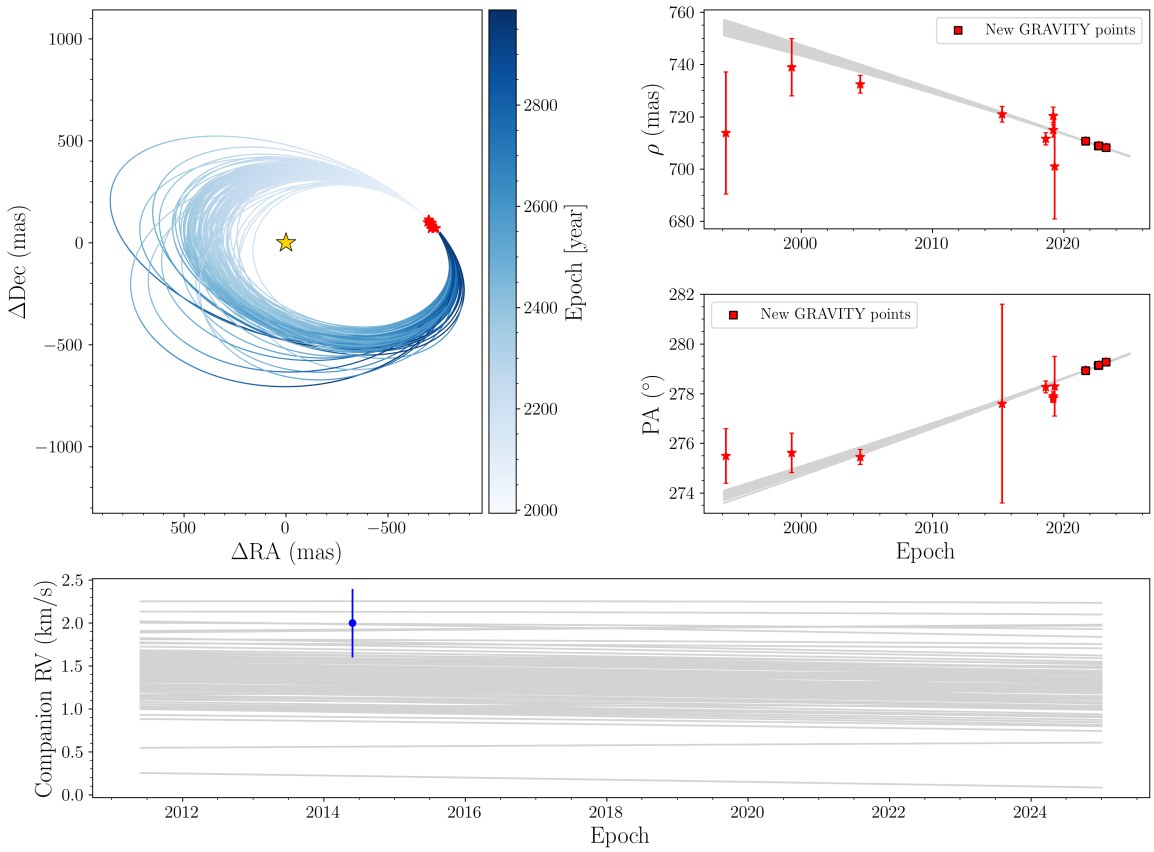

Figure 1. Orbit fit for Case `GRAVLowRV` (see Table 5), using astrometry including GRAVITY data and low-precision radial velocity measurement. The plot shows posterior samples from the orbit fit for GQ Lup B, generated using `orbitize!`. Blue ellipses represent 100 orbits randomly drawn from the posterior, and red points indicate the relative astrometric data. In the right panels, red points correspond to astrometric measurements from both the literature and new GRAVITY data included in the fit; gray lines trace the same 100 posterior orbits in separation and position angle. The results illustrate the power of GRAVITY data in improving the orbit solution for GQ Lup B.

Table 5
Overview of Dataset Combinations Used for the Orbital Fitting

Code	Data Used	Literature Astrometry	GRAVITY (This Work)	RV
`NoGRAVNoRV`	Astrometry only (no GRAVITY, no RV)	✓	…	…
`GRAVNoRv`	Astrometry + GRAVITY (no RV)	✓	✓	…
`NoGRAVLowRV`	Astrometry (no GRAVITY) + Low-precision RV[a]	✓	…	✓
`NoGRAVHighRV`	Astrometry (no GRAVITY) + High-precision RV[b]	✓	…	✓
`GRAVLowRV`	Astrometry + GRAVITY + Low-precision RV (Adopted)[a]	✓	✓	✓
`GRAVHighRV`	Astrometry + GRAVITY + High-precision RV[b]	✓	✓	✓

Notes.
[a] From H. Schwarz et al. (2016).
[b] From D. González Picos et al. (2025).

315° ± 4° (C. Lazzoni et al. 2020) and the circumstellar disk, which peaks at 346° ± 1° (M. A. MacGregor et al. 2017). The star's Ω is unknown and is assumed to be uniform between 0° and 360°, as shown by the yellow line.

We use equations from B. P. Bowler et al. (2023) to calculate the mutual inclination between our adopted planet fit and the circumstellar disk, the stellar spin axis, and also the disk of GQ Lup C. The bottom panel shows that GQ Lup B appears misaligned with both the disk by 63^{+6}_{-14}° and 52^{+19}_{-24}° with the stellar spin, confirming a misaligned configuration. The mutual inclination between GQ Lup B and the disk of GQ Lup C is smaller, peaking at 35^{+6}_{-13}°.

5. Discussion

Our results are consistent with the eccentricity and inclination calculations from T. Stolker et al. (2021), where they combine RV measurements from H. Schwarz et al. (2016) with astrometry from VLT/NACO and VLT/MUSE. They report an eccentricity and inclination constraint of $0.24^{+0.32}_{-0.17}$

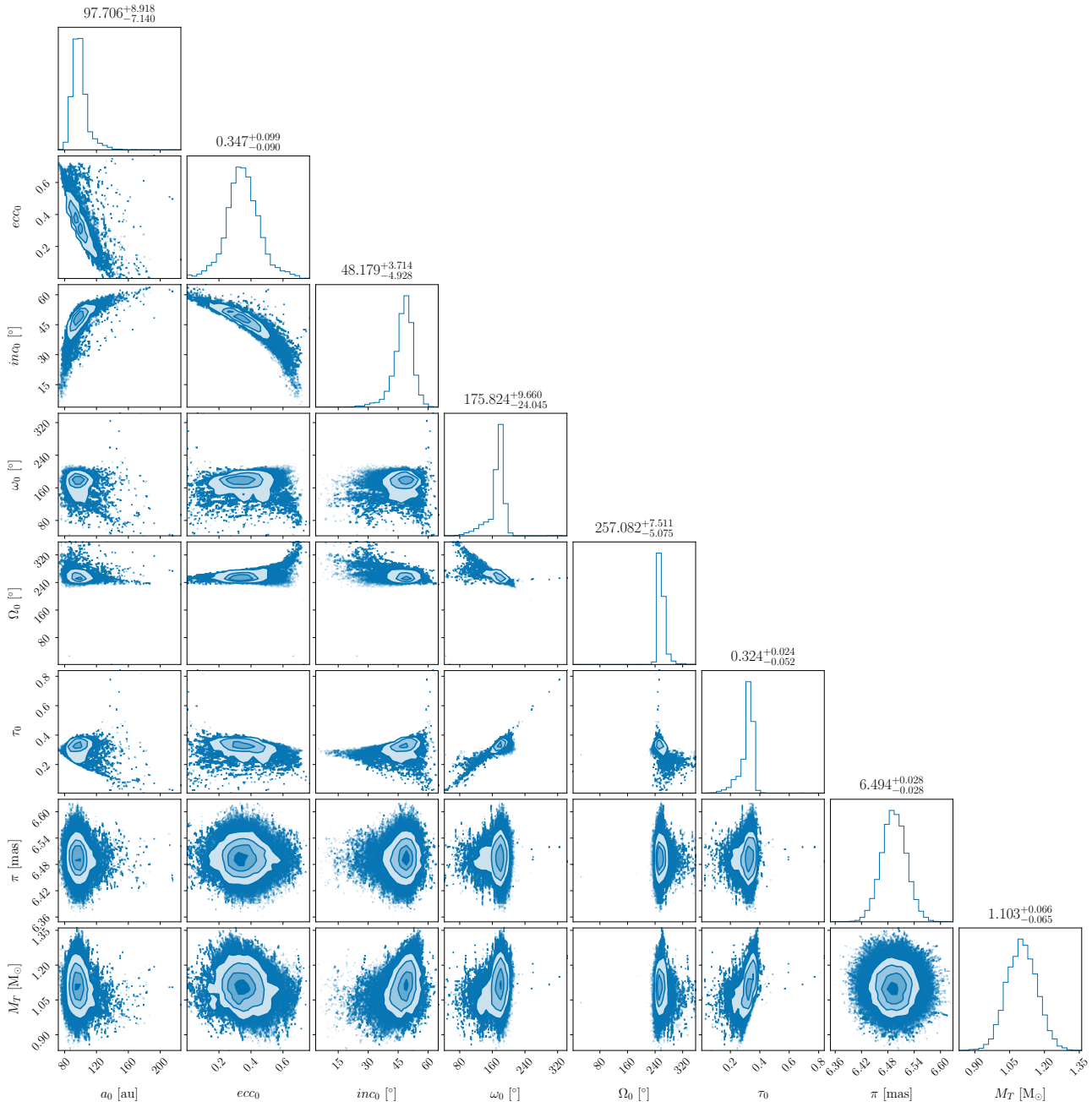

Figure 2. Corner plot of the posterior distributions for Case GRAVLowRV (see Table 5), which includes all available astrometry (including GRAVITY) and low-precision radial velocity measurement. The contours represent the 1σ, 2σ, and 3σ credible intervals, with individual posterior samples beyond the 3σ level shown as blue points. Strong covariances between eccentricity, inclination, and semimajor axis are apparent.

and 60^{+5}_{-9} compared to $0.35^{+0.10}_{-0.09}$ and $48.2^{+3.7}_{-4.9}$ in this work. Moreover, they find a mutual inclination of 84^{+9}_{-9} between the orbit of the companion and the circumstellar disk compared to our constraint of 63^{+6}_{-14}. By incorporating high-precision GRAVITY astrometry, we have tightened these constraints with reduced errors on both eccentricity and inclination compared to T. Stolker et al. (2021).

The formation pathway for GQ Lup B has remained elusive since its discovery. R. Neuhauser et al. (2005) argued for a formation scenario consistent with cloud formation, which appears consistent with the presence of a compact circumstellar disk imaged by ALMA; such a disk could be too small to have formed GQ Lup B in situ (M. A. MacGregor et al. 2017). More recently, T. Stolker et al. (2021) found the disk to be significantly misaligned with the orbit, suggesting a history of dynamic interactions or cloud fragmentation. Complementary to the architectural constraints, the consistent chemical compositions of GQ Lup A and B point toward formation via cloud fragmentation (D. Stamatellos et al. 2007; D. Stamatellos & A. P. Whitworth 2009). Our analysis leverages the power of VLT/GRAVITY astrometry and high-precision spectroscopy from CRIRES+ to provide precise and

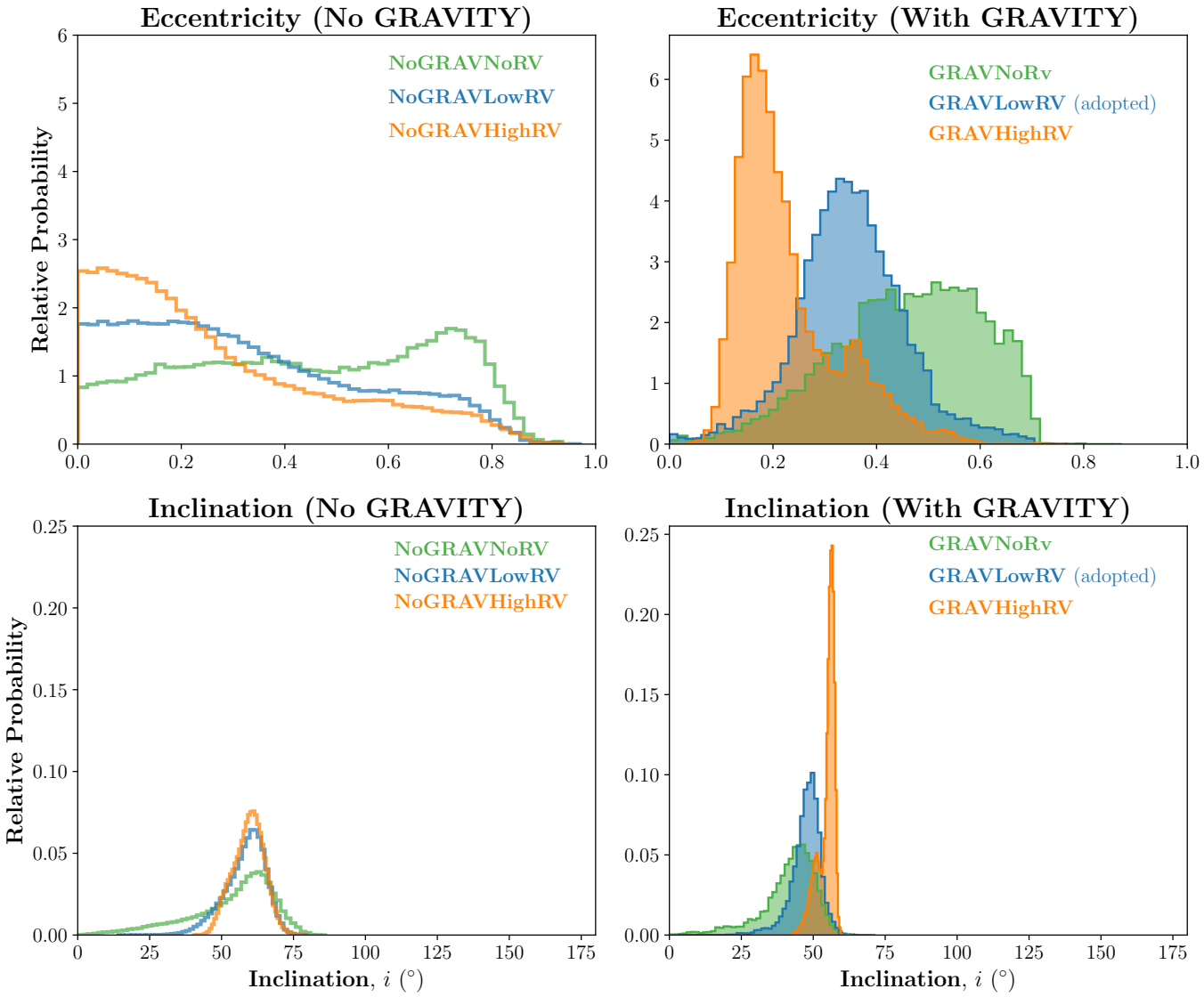

Figure 3. Posterior eccentricity and inclination distributions for GQ Lup B based on six orbital fits (see Table 5), grouped by inclusion of GRAVITY astrometry. The histograms show the relative probability of eccentricity and inclination values. Inclusion of GRAVITY and relative RV measurements substantially tightens the constraints. While the high-precision RV case (orange) provides the narrowest distribution, it may be biased due to stellar variability or unresolved companions. The adopted blue case (`GRAVLowRV`) incorporates GRAVITY astrometry and low-precision RV, offering a robust and physically plausible solution consistent with a moderately eccentric and inclined orbit.

robust estimates of the orbit and favors the expectations from dynamically hot in situ formation processes like cloud fragmentation.

We have shown that when we combine high-precision astrometry from GRAVITY and high-precision spectroscopy from CRIRES+, we can precisely constrain 3D orbits of planets at ∼100 au. For the case of GQ Lup B, the addition of planetary RVs—despite our cautious adoption of the lower-precision dataset—has significantly improved constraints on the planet's orbit. The moderate eccentricity ($e \sim 0.35$) and well-localized inclination (near $48^{+3.7}_{-4.9}$°) are now less strongly degenerate. The resulting orbital solution places the planet between the inner circumstellar disk (truncated at ∼50–75 au) and the wide companion GQ Lup C (projected separation ∼2400 au).

The orbital architecture of the GQ Lup system points to a dynamically complex history. The orbital plane of GQ Lup B ($i = \simeq 48.^{\circ}6$) is likely misaligned with both the stellar spin axis ($i \simeq 26.^{\circ}6$) and the circumstellar disk ($i \simeq 60.^{\circ}5$), disfavoring a formation via coplanar, in situ core accretion. Interestingly, although GQ Lup B is misaligned with the primary disk, its inclination is roughly consistent with that of GQ Lup C. The similarity in inclination and longitude of ascending node—though still uncertain—experienced similar early dynamical shaping. Dynamical simulations of the system's formation could help shed light on which of these scenarios is most likely.

Using the posterior distributions from our adopted orbital solution (Fit `GRAVLowRV`), we find a pericenter distance of 65^{+15}_{-14} au. The disk, as observed by ALMA and presented in M. A. MacGregor et al. (2017), appears smooth and symmetric out to an outer radius of ∼50 au. Additionally, the polarimetry results also show potential spiral structure in the disk (R. G. van Holstein et al. 2021), which can be caused due to the pericenter distance. We estimated that the half-width of the chaotic zone can be estimated using the expression from

Table 6
Posterior Medians and 1σ Uncertainties for Orbital Parameters under Six Fitting Configurations

Parameter	NoGRAVNoRV	GRAVNoRV	NoGRAVLowRV	NoGRAVHighRV	GRAVLowRV	GRAVHighRV
SMA (au)	$112.45^{+74.30}_{-34.25}$	$98.94^{+11.43}_{-10.80}$	$112.97^{+28.38}_{-22.17}$	$114.25^{+22.93}_{-17.61}$	$97.71^{+8.92}_{-7.14}$	$106.55^{+5.59}_{-5.53}$
e	$0.46^{+0.27}_{-0.29}$	$0.47^{+0.14}_{-0.16}$	$0.28^{+0.31}_{-0.19}$	$0.21^{+0.32}_{-0.15}$	$0.35^{+0.10}_{-0.09}$	$0.20^{+0.14}_{-0.06}$
i (deg)	$57.43^{+9.40}_{-19.18}$	$43.52^{+6.42}_{-9.62}$	$59.24^{+5.60}_{-8.22}$	$59.73^{+4.97}_{-6.16}$	$48.18^{+3.71}_{-4.93}$	$55.67^{+1.45}_{-4.32}$
ω_0 (deg)	$190.94^{+96.26}_{-134.68}$	$196.51^{+20.05}_{-23.57}$	$166.23^{+116.69}_{-69.14}$	$164.14^{+132.94}_{-57.28}$	$175.82^{+9.66}_{-24.05}$	$161.25^{+13.53}_{-37.91}$
Ω_0 (deg)	$199.04^{+69.34}_{-135.95}$	$241.01^{+15.53}_{-23.66}$	$266.54^{+21.09}_{-11.36}$	$265.51^{+20.25}_{-5.91}$	$257.08^{+7.51}_{-5.08}$	$263.74^{+8.81}_{-2.25}$
τ_0	$0.36^{+0.26}_{-0.16}$	$0.30^{+0.03}_{-0.05}$	$0.37^{+0.36}_{-0.19}$	$0.37^{+0.41}_{-0.19}$	$0.32^{+0.02}_{-0.05}$	$0.33^{+0.04}_{-0.12}$
π (mas)	$6.49^{+0.03}_{-0.03}$	$6.49^{+0.03}_{-0.03}$	$6.49^{+0.03}_{-0.03}$	$6.49^{+0.03}_{-0.03}$	$6.49^{+0.03}_{-0.03}$	$6.51^{+0.03}_{-0.03}$
$M_{\rm tot}$ ($M_\odot$)	$1.05^{+0.07}_{-0.07}$	$1.06^{+0.07}_{-0.07}$	$1.05^{+0.07}_{-0.07}$	$1.04^{+0.07}_{-0.07}$	$1.10^{+0.07}_{-0.06}$	$1.28^{+0.07}_{-0.15}$

Note. Parameters shown are: a—semimajor axis (au); e—eccentricity; i—inclination (deg); ω_P—argument of periastron (deg); Ω—longitude of ascending node (deg); τ_0—normalized epoch of periastron; π—parallax (mas); and $M_{\rm tot}$—total system mass ($M_\odot$) for all six cases.

S. Morrison & R. Malhotra (2015),

$$\Delta a \approx 1.5\ \mu^{0.28}\ a_p, \tag{1}$$

where

1. Δa is the half-width of the chaotic zone.
2. a_p is the semimajor axis of the companion.
3. $\mu = \frac{M_p}{M_*}$ is the mass ratio of the companion (M_p) to the host star (M_*).

We find the chaotic zone to extend from 49.8 to 150.2 au, indicating that the companion can dynamically truncate or sculpt the disk. Our calculated pericenter distance of 65^{+15}_{-14} au lies well within this zone, and because the polarimetry reveals a warp at similar radii, it is possible that the companion is truncating and warping the inner edge of the disk.

We also assessed the plausibility of Kozai–Lidov (KL) oscillations induced by the outer companion GQ Lup C. Assuming a circular orbit at 2300 au and component masses of $1\,M_\odot$ (GQ Lup A), $20\,M_{\rm Jup}$ (GQ Lup B), and $0.15\,M_\odot$ (GQ Lup C), we estimate a KL timescale of approximately 82 Myr. This was calculated using the quadrupole-order approximation for hierarchical triples (J. M. O. Antognini 2015),

$$t_{\rm KL} \approx \frac{M_{\rm A} + M_{\rm B}}{M_{\rm C}} \cdot \frac{P_{\rm C}^2}{P_{\rm B}} \cdot (1 - e_{\rm C}^2)^{3/2}, \tag{2}$$

where $P_{\rm B}$ and $P_{\rm C}$ are the orbital periods of the inner and outer binaries, respectively. This timescale is much longer than the estimated age of the system (∼1–5 Myr), suggesting that secular interactions from GQ Lup C are unlikely to have played a significant role in shaping its current orbit but could become dynamically relevant over the system's lifetime.

Dynamical scattering is unlikely. GQ Lup B could be the inner survivor of a past interaction that ejected a lower-mass object, possibly on the order of a few Jupiter masses. Conversely, GQ Lup B could be the outer object resulting from scattering by an unseen, more massive inner perturber. However, the smooth morphology of the disk argues against the presence of such a companion in the inner few tens of astronomical units. We also find no evidence of a transition disk or inner cavity in the current literature, though further imaging could help clarify this point. If GQ Lup A were a close binary, that would likely be visible in the RVs of the primary. Atmospheric constraints also point to dynamical scattering as a less probable scenario.

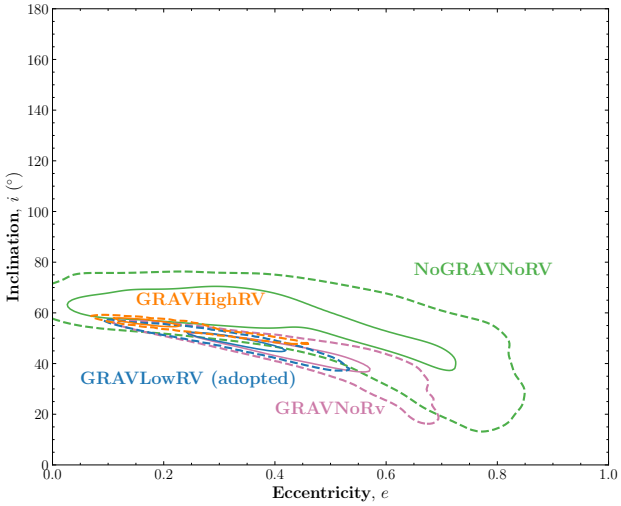

Figure 4. 1σ and 2σ joint posterior distributions of eccentricity and inclination for GQ Lup B under four cases (see Table 5) are shown by lines and dashed lines, respectively. The inclusion of GRAVITY astrometry significantly narrows the orbital parameter space, particularly by reducing the volume of the joint eccentricity–inclination posterior. Adding radial velocity measurements —especially in the GRAVLowRV and GRAVHighRV cases—further sharpens the constraints by reducing the eccentricity–inclination degeneracy, yielding a well-localized solution consistent with a moderately eccentric orbit.

Flyby interactions are unlikely in this case. While GQ Lup shares proper motion characteristics with core members of the Lupus star-forming region—suggesting it is not an interloper —this alone does not rule out the possibility of a past stellar encounter. However, the continued presence of the wide tertiary companion, GQ Lup C, at a projected separation of ∼2400 au places strong constraints on the severity of any potential flyby. A sufficiently close or energetic encounter capable of exciting the observed eccentricity or inclination would likely have disrupted the outer companion, making such a scenario implausible.

The constraints suggest that GQ Lup B likely formed via cloud fragmentation with very minimal dynamical reshaping. The KL timescale exceeds the age of the system, making significant excitation unlikely. The inner companion's orbit is misaligned with the disk, consistent with primordial tilt imparted at formation rather than due to later perturbations. The inner companion has a moderate, not extreme, eccentricity, and matched expectation for cloud collapse, and argues against violent scattering events. Overall, our calculations

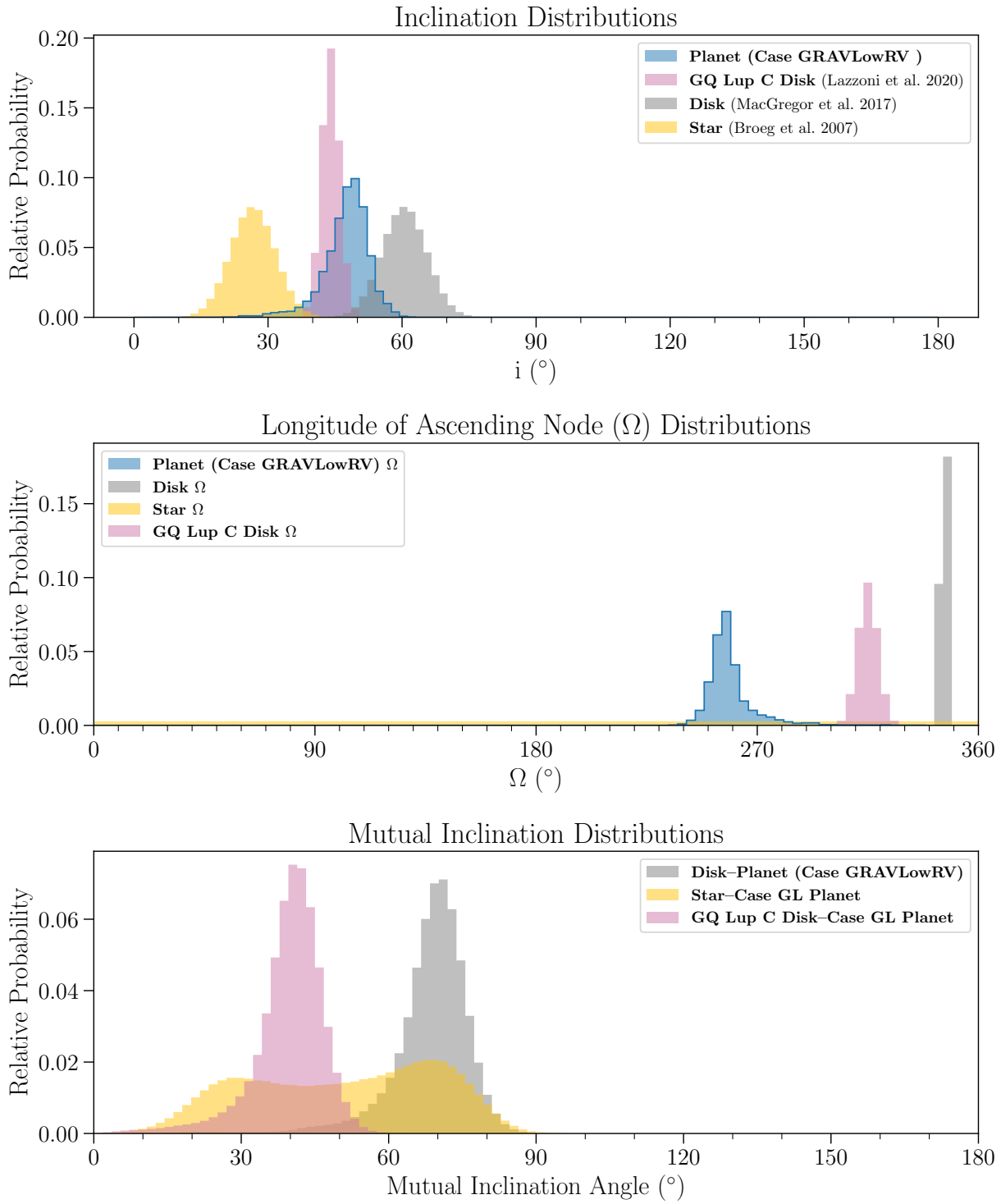

Figure 5. Inclination and longitude of ascending node (Ω) distributions for the `GRAVLowRV`-case orbit of GQ Lup B (blue), compared against the circumstellar disk (M. A. MacGregor et al. 2017), stellar spin axis (C. Broeg et al. 2007), and GQ Lup C's disk (C. Lazzoni et al. 2020). The bottom panel shows the mutual inclination angle between the planet and each reference plane.

support a formation scenario that is dominated by cloud fragmentation.

6. Conclusions

In this work, we combine the high-precision astrometric measurements from GRAVITY, SPHERE, and NACO with high-resolution ($R \sim 100{,}000$) spectroscopic data from CRIRES+ to refine the orbit of GQ Lup B. While we adopt the lower-precision RV data set from H. Schwarz et al. (2016) due to concerns about unmodeled systematics in higher-precision measurements (e.g., stellar activity or an unresolved companion), even this modest precision measurement ($2.03 \pm 0.4\,\mathrm{km\,s^{-1}}$)—when combined with interferometric astrometry—proves powerful. It helps break the known degeneracy between inclination and eccentricity in long-period, astrometry-only orbits, allowing us to obtain the first well-

constrained eccentricity posterior for GQ Lup B. Specifically, the eccentricity is refined from $0.47^{+0.14}_{-0.16}$ (GRAVITY-only) to $0.35^{+0.10}_{-0.09}$ with the inclusion of RVs and GRAVITY data.

Beyond orbital parameter estimation, we explore the 3D architecture of the system by computing the mutual inclinations between GQ Lup B, the stellar spin axis, the circumstellar disk, and the wide companion GQ Lup C. We find that GQ Lup B is misaligned with the inner system—both the disk and stellar spin axis—but comparatively more aligned with the disk of GQ Lup C. This configuration suggests that GQ Lup B may have formed via cloud fragmentation, and its misalignment with the outer disk is coincidental.

Our results underscore how the combination of high-precision astrometry and planetary RVs enables significantly more robust orbital constraints for wide-orbit companions. This technique is particularly valuable in systems like GQ Lup, where traditional core accretion models are challenged and observational baselines are short. As high-resolution spectroscopic techniques continue to mature and as instruments like GRAVITY and CRIRES+ expand their reach, we are entering an era where joint astrometry–RV analysis will allow us to uncover population-level trends between inclination and eccentricity, and formation pathways, ultimately building a holistic understanding of the orbits of companions at wide separations.

Acknowledgments

Based on observations collected at the European Southern Observatory under ESO programmes: PI: Sylvestre Lacour, 1104.C-0651, 109.238N.001, and 109.238N.002.

V.V. acknowledges support from the NASA FINESST Fellowship under award number 80NSSC21K1852, the University of California, Irvine's Graduate Dean's Dissertation Fellowship, and additional funding support from UCI. . V. V. extends sincere thanks to Ruth Murray-Clay for her valuable insights. V.V. would like to thank Paul Robertson and his group members for valuable discussions, as well as the members of Jason Wang's BOBA group. S.L. acknowledges the support of the French Agence Nationale de la Recherche (ANR-21-CE31-0017, ExoVLTI) and of the European Research Council (ERC Advanced grant No. 101142746, PLANETES). J.J.W. and A.C. are supported by NASA XRP Grant 80NSSC23K0280. Based on observations collected at the European Southern Observatory under ESO programmes 1104.C-0651 and 109.238N.001.

The authors acknowledge the use of OpenAI's ChatGPT for assistance with proofreading and visualization suggestions during the preparation of this manuscript. All scientific content and interpretations come from the authors.

Data Availability

The code for generating the plots and additional corner and orbit plots for the other five cases is available on Zenodo at doi:10.5281/zenodo.17087542, and GitHub (https://github.com/astrovidee/GQ_Lup_B_analysis_2025). The orbit chains for GQ Lup B will also be added to whereistheplanet.com (J. J. Wang et al. 2021).

Facility: VLTI (GRAVITY).

Software: `numpy` (C. R. Harris et al. 2020), `pandas` (W. McKinney 2010), `matplotlib` (J. D. Hunter 2007), `corner` (D. Foreman-Mackey 2016), `scipy` (P. Virtanen et al. 2020), `astropy` (Astropy Collaboration et al. 2013, 2018, 2022), `orbitize!` (S. Blunt et al. 2020, `Aspro` (https://www.jmmc.fr/english/tools/proposal-preparation/aspro; L. Bourgès & G. Duvert 2016).

For proofreading: ChatGPT (OpenAI 2023).

ORCID iDs

Vidya Venkatesan https://orcid.org/0000-0002-5638-4344
S. Blunt https://orcid.org/0000-0002-3199-2888
G.-D. Marleau https://orcid.org/0000-0002-2919-7500
R. Genzel https://orcid.org/0000-0002-2767-9653
S. Gillessen https://orcid.org/0000-0002-5708-0481
J. H. Girard https://orcid.org/0000-0001-8627-0404
S. Grant https://orcid.org/0000-0002-3499-8142
Th. Henning https://orcid.org/0000-0002-1493-300X
S. Hinkley https://orcid.org/0000-0001-8074-2562
S. Hippler https://orcid.org/0000-0002-3912-6108
L. Kreidberg https://orcid.org/0000-0003-0514-1147
N. T. Kurtovic https://orcid.org/0000-0002-2358-4796
J.-B. Le Bouquin https://orcid.org/0000-0002-0493-4674
D. Lutz https://orcid.org/0000-0003-0291-9582
A. Mérand https://orcid.org/0000-0003-2125-0183
C. Mordasini https://orcid.org/0000-0002-1013-2811
T. Ott https://orcid.org/0000-0003-1572-0396
T. Paumard https://orcid.org/0000-0003-0655-0452
G. Perrin https://orcid.org/0000-0003-0680-0167
S. Petrus https://orcid.org/0000-0003-0331-3654
Z. Rustamkulov https://orcid.org/0000-0003-4408-0463
J. Shangguan https://orcid.org/0000-0002-4569-9009
A. Shields https://orcid.org/0000-0002-7086-9516
O. Straub https://orcid.org/0000-0001-5755-0677
C. Straubmeier https://orcid.org/0000-0002-0671-9302
E. Sturm https://orcid.org/0000-0002-0018-3666
L. J. Tacconi https://orcid.org/0000-0002-1485-9401
A. Vigan https://orcid.org/0000-0002-5902-7828
F. Vincent https://orcid.org/0000-0002-3855-0708
J. Woillez https://orcid.org/0000-0002-2958-4738

References

Alcalá, J. M., Majidi, F. Z., Desidera, S., et al. 2020, A&A, 635, L1
Antognini, J. M. O. 2015, MNRAS, 452, 3610
Astropy Collaboration, Price-Whelan, A. M., Lim, P. L., et al. 2022, ApJ, 935, 167
Astropy Collaboration, Price-Whelan, A. M., Sipőcz, B. M., et al. 2018, AJ, 156, 123
Astropy Collaboration, Robitaille, T. P., Tollerud, E. J., et al. 2013, A&A, 558, A33
Balmer, W. O., Franson, K., Chomez, A., et al. 2025, AJ, 169, 30
Balmer, W. O., Pueyo, L., Lacour, S., et al. 2024, AJ, 167, 64
Blunt, S., Balmer, W. O., Wang, J. J., et al. 2023, AJ, 166, 257
Blunt, S., Wang, J. J., Angelo, I., et al. 2020, AJ, 159, 89
Boss, A. P. 1997, Sci, 276, 1836
Bourgès, L., & Duvert, G. 2016, Proc. SPIE, 9907, 990711
Bowler, B. P., Blunt, S. C., & Nielsen, E. L. 2020, AJ, 159, 63
Bowler, B. P., Tran, Q. H., Zhang, Z., et al. 2023, AJ, 165, 164
Brandt, G. M., Brandt, T. D., Dupuy, T. J., Li, Y., & Michalik, D. 2021, AJ, 161, 179
Broeg, C., Schmidt, T. O. B., & Guenther, E. W. 2007, yCat, 346, 81039
Bryan, M. L., Howard, A. W., Kataria, T., et al. 2021, AJ, 162, 81
Bryan, M. L., Knutson, H. A., Howard, A. W., et al. 2016, ApJ, 821, 89
Chabrier, G. 2003, PASP, 115, 763
Crida, A., Masset, F., & Morbidelli, A. 2009, ApJL, 705, L148
Cugno, G., Patapis, P., Banzatti, A., et al. 2024, ApJL, 966, L21
De Rosa, R. J., Dawson, R., & Nielsen, E. L. 2020, A&A, 640, A73
Donati, J. F., Gregory, S. G., Alencar, S. H. P., et al. 2012, MNRAS, 425, 2948

Dong, R., Vorobyov, E., Pavlyuchenkov, Y., Chiang, E., & Liu, H. B. 2016, ApJ, 823, 141
Do O, C. R., O'Neil, K. K., Konopacky, Q. M., et al. 2023, AJ, 166, 48
Ferrer-Chávez, R., Wang, J. J., & Blunt, S. 2021, AJ, 161, 241
Foreman-Mackey, D. 2016, JOSS, 1, 24
Foreman-Mackey, D., Hogg, D. W., Lang, D., & Goodman, J. 2013, PASP, 125, 306
Gaia Collaboration, Vallenari, A., Brown, A. G. A., et al. 2023, A&A, 674, A1
González Picos, D., Snellen, I. A. G., de Regt, S., et al. 2025, A&A, 693, A298
GRAVITY Collaboration, Nowak, M., Lacour, S., et al. 2020, A&A, 633, A110
Harris, C. R., Millman, K. J., van der Walt, S. J., et al. 2020, Natur, 585, 357
Holmberg, M., & Madhusudhan, N. 2022, AJ, 164, 79
Horstman, K., Ruffio, J.-B., Batygin, K., et al. 2024, AJ, 168, 175
Hunter, J. D. 2007, CSE, 9, 90
Ikoma, M., & Kobayashi, H. 2025, ARA&A, 63, 217
Inaba, S., Wetherill, G. W., & Ikoma, M. 2003, Icar, 166, 46
Janson, M., Brandner, W., Henning, T., & Zinnecker, H. 2006, A&A, 453, 609
Kammerer, J., Lacour, S., Stolker, T., et al. 2021, A&A, 652, A57
Kratter, K., & Lodato, G. 2016, ARA&A, 54, 271
Lacour, S., Wang, J. J., Nowak, M., et al. 2020, Proc. SPIE, 11446, 114460O
Lazzoni, C., Vigan, A., Gratton, R., et al. 2020, A&A, 638, A20
MacGregor, M. A., Wilner, D. J., Czekala, I., et al. 2017, ApJ, 835, 17
Marleau, G.-D., Coleman, G. A. L., Leleu, A., & Mordasini, C. 2019, A&A, 624, A20
Marois, C., Macintosh, B., & Barman, T. 2007, ApJL, 654, L151
Mayer, L., Quinn, T., Wadsley, J., & Stadel, J. 2002, Sci, 298, 1756
McKinney, W. 2010, in Proc. 9th Python in Science Conf., ed. S. van der Walt & J. Millman (Austin, TX: SciPy), 56
Morrison, S., & Malhotra, R. 2015, ApJ, 799, 41
Nagpal, V., Blunt, S., Bowler, B. P., et al. 2023, AJ, 165, 32
National Academies of Sciences, Engineering, and Medicine 2023, Pathways to Discovery in Astronomy and Astrophysics for the 2020s (Washington, DC: The National Academies Press)
Nayakshin, S. 2017, PASA, 34, e002
Neuhauser, R., Guenther, E. W., Wuchterl, G., et al. 2005, A&A, 435, L13
Nowak, M., Lacour, S., Abuter, R., et al. 2024, A&A, 687, A248
OpenAI, 2023 ChatGPT (Mar 14 version) [Large Language Model], https://chat.openai.com
Pollack, J. B., Hubickyj, O., Bodenheimer, P., et al. 1996, Icar, 124, 62
Reggiani, M., Meyer, M. R., Chauvin, G., et al. 2016, A&A, 586, A147
Schwarz, H., Ginski, C., de Kok, R. J., et al. 2016, A&A, 593, A74
Stamatellos, D., Hubber, D. A., & Whitworth, A. P. 2007, MNRAS, 382 L30
Stamatellos, D., & Whitworth, A. P. 2009, MNRAS, 392, 413
Stevenson, A. T., Haswell, C. A., Barnes, J. R., & Barstow, J. K. 2023, MNRAS, 526, 5155
Stolker, T., Haffert, S. Y., Kesseli, A. Y., et al. 2021, AJ, 162, 286
van Holstein, R. G., Stolker, T., Jensen-Clem, R., et al. 2021, A&A, 647 A21
Venkatesan, V., Shields, A. L., Deitrick, R., Wolf, E. T., & Rushby, A. 2025, AsBio, 25, 42
Veras, D., Crepp, J. R., & Ford, E. B. 2009, ApJ, 696, 1600
Virtanen, P., Gommers, R., Oliphant, T. E., et al. 2020, NatMe, 17, 261
Vousden, W. D., Farr, W. M., & Mandel, I. 2016, MNRAS, 455, 1919
Winterhalder, T. O., Kammerer, J., Lacour, S., et al. 2025, A&A, 700, A4
Wu, Y.-L., Sheehan, P. D., Males, J. R., et al. 2017, ApJ, 836, 223
Xuan, J. W., Hsu, C.-C., Wang, J. J., et al. 2024, Natur, 634 1070
Wang, J. J., Kulikauskas, M., & Blunt, S., 2021 whereistheplanet: Predicting positions of directly imaged companions, Astrophysics Source Code Library, ascl:2101.003
Xuan, J. W., Wang, J., Ruffio, J.-B., et al. 2022, ApJ, 937, 54